Published in final edited form as:
Neuroimage. 2009 February 1; 44(3): 653–660. doi:10.1016/j.neuroimage.2008.09.027.

Differentiation between Glioblastomas and Solitary Brain Metastases Using Diffusion Tensor Imaging

Sumei Wang[1], **Sungheon Kim**[1,*], **Sanjeev Chawla**[1], **Ronald L. Wolf**[1], **Wei-Guo Zhang**[1,3], **Donald M. O'Rourke**[2], **Kevin D. Judy**[2], **Elias R. Melhem**[1], and **Harish Poptani**[1]

1 *Department of Radiology, Division of Neuroradiology, Hospital of the University of Pennsylvania, 3400 Spruce Street, Philadelphia, PA 19104, USA*

2 *Department Neurosurgery, Hospital of the University of Pennsylvania, 3400 Spruce Street, Philadelphia, PA 19104, USA*

3 *Department of Radiology, Daping Hospital, 10 Changjiang Zhilu, Chongqing 400042, China*

Abstract

The purpose of this study is to determine whether diffusion tensor imaging (DTI) metrics including tensor shape measures such as linear and planar anisotropy coefficients (CL and CP) can help differentiate glioblastomas from solitary brain metastases. Sixty-three patients with histopathologic diagnosis of glioblastomas (22 men, 16 women, mean age 58.4 years) and brain metastases (13 men, 12 women, mean age 56.3 years) were included in this study. Contrast-enhanced T1-weighted, fluid attenuated inversion recovery (FLAIR) images, fractional anisotropy (FA), apparent diffusion coefficient (ADC), CL and CP maps were co-registered and each lesion was semi-automatically subdivided into four regions: central, enhancing, immediate peritumoral and distant peritumoral. DTI metrics as well as the normalized signal intensity from the contrast-enhanced T1-weighted images were measured from each region. Univariate and multivariate logistic regression analyses were employed to determine the best model for classification. The results demonstrated that FA, CL and CP from glioblastomas were significantly higher than those of brain metastases from all segmented regions ($p < 0.05$), and the differences from the enhancing regions were most significant ($p < 0.001$). FA and CL from the enhancing region had the highest prediction accuracy when used alone with an area under the curve of 0.90. The best logistic regression model included three parameters (ADC, FA and CP) from the enhancing part, resulting in 92% sensitivity, 100% specificity and area under the curve of 0.98. We conclude that DTI metrics, used individually or combined, have a potential as a noninvasive measure to differentiate glioblastomas from metastases.

Introduction

Glioblastomas and brain metastases (according to the WHO 2007 classification) are the two most common brain neoplasms in adults (Louis et al., 2007). The management of these two neoplasms is vastly different and can potentially affect the clinical outcome (Giese and

Corresponding author: Sungheon Kim, PhD, Department of Radiology, Hospital of the University of Pennsylvania, 423 Guardian Drive, Blockley Hall-B6, Philadelphia, PA 19104, USA, Phone: (215) 746-7387, Fax: (215) 573-2113, E-mail: Sungheon.Kim@uphs.upenn.edu.

A portion of this work was presented at the 16th annual meeting of ISMRM, Toronto, Canada, 2008.

Westphal, 2001; Soffietti et al., 2002). In general, differentiation of these two neoplasms is possible based on the clinical history or presence of multiple enhancing lesions (Tang et al., 2006; Zhang and Olsson, 1997). However, distinction remains challenging when the patient presents with a solitary enhancing mass as both glioblastomas and metastases may exhibit ring-enhancement and extensive edema on magnetic resonance imaging (MRI) (Schiff, 2001). In addition, a solitary brain mass may be the first manifestation of disease in about 30% of patients with systemic cancer (Schiff, 2001).

Diffusion tensor imaging (DTI) has been used to study pathologic changes in brain tumors (Field et al., 2004; Rumboldt et al., 2006; Stadlbauer et al., 2006; Yamasaki et al., 2005). It has also been applied in differentiating glioblastomas from metastases, however, with mixed results (Calli et al., 2006; Lu et al., 2003; Lu et al., 2004; Morita et al., 2005; Oh et al., 2005; Tsuchiya et al., 2005; Yamasaki et al., 2005). Some reports have suggested that apparent diffusion coefficient (ADC) (Lu et al., 2003; Lu et al., 2004; Morita et al., 2005) and fractional anisotropy (FA) (Lu et al., 2004) are helpful for the differentiation, while others indicated the limited use of ADC (Calli et al., 2006; Oh et al., 2005; Yamasaki et al., 2005) and FA (Lu et al., 2003; Tsuchiya et al., 2005) for the differentiation. These conflicting results may be due to the differences in acquisition and analytical methods employed, achievable signal to noise ratio (SNR), gradient directions used, motion and eddy current artifacts that are typically observed on DTI images as well as the heterogeneous nature of brain neoplasm.

Most earlier DTI studies have focused on the peritumoral region that lies just outside the contrast-enhancing region for detection of differences in tumor infiltration between glioblastomas and metastases (Cha, 2006; Lu et al., 2003; Lu et al., 2004; Morita et al., 2005). However, to date, there has been no report on systemic measurements of DTI metrics from different regions of the tumor, which might be a more robust way of characterizing brain neoplasms. The enhancing neoplastic mass can be generally categorized into two sub-regions with the contrast-enhancing region representing the solid part of the tumor, while the central area with no or slight enhancement representing necrotic or cystic part of the tumor. Similarly, the edematous region can also be separated into two categories with regions surrounding the enhancing part of the tumor potentially including infiltrative tumor cells, and the more distal regions mainly comprised of vasogenic edema.

ADC and FA constitute only a fraction of the information available from DTI measurements. More detailed features of the tensor shape, such as linear and planar anisotropy coefficients (CL and CP) (Alexander et al., 2000; Westin et al., 2002; Westin et al., 1997) may further elucidate tissue characterization as previously reported for brain tumors (Kim et al., 2007).

Therefore, in this study, we hypothesized that diffusion characteristics including CL and CP of glioblastomas are different from brain metastases in different regions of the tumor, such as ring-enhancing, central (non or less) enhancing, immediate and distant peritumoral regions. We also hypothesized that these two tumor types can be differentiated based on the DTI metrics measured from one or more of these sub-regions of the tumor. In order to achieve this goal, we developed a semi-automated segmentation method to delineate different regions of the tumor based on conventional MRI. DTI metrics from segmented regions were combined to generate an optimal regression model to differentiate these two tumors.

Materials and Methods

Patients

Sixty-three patients with solitary enhancing lesions, based on contrast-enhanced (CE) T1-weighted images, were recruited from our institution between June 2006 and September 2007. Patients with multiple brain lesions, nonenhancing tumor, or clinical history of any prior

therapy to the brain were not included. The study was approved by the Institutional Review Board and was compliant with the Health Insurance Portability and Accountability Act (HIPAA).

All patients underwent gross total or near total resection of the enhancing tumor. Histopathologic analysis of the resected tissue confirmed the diagnosis of glioblastoma in 38 patients (22 men, 16 women, age range 28–75 years, mean age 58.4 years ± 11.4 [standard deviation]) and brain metastasis in 25 patients (13 men, 12 women, age range 40–80 years, mean age 56.3 years ± 12.2). The primary cancer types for patients with metastatic lesions are presented in Table 1.

Data acquisition

MR studies were performed on a Siemens Tim Trio 3.0 T whole body scanner (Siemens, Erlangen, Germany) using a 12-channel phased-array head coil. Routine MR pulse sequences included axial T_1-weighted 3-D magnetization prepared rapid acquisition gradient-echo (MPRAGE) (TR/TE 1760/3.1, 192 × 256 matrix size, 1mm slice thickness) and axial fast fluid-attenuated inversion recovery (FLAIR) (TR/TE/TI 9420/141/2500, 3mm slice thickness) images. DTI data was acquired using a 12 direction single shot; spin echo - echo planar imaging (EPI) sequence with parallel imaging using generalized autocalibrating partially parallel acquisition (GRAPPA) and acceleration factor of 2. Sequence parameters used were: TR/TE = 4900/83, NEX = 6, field of view (FOV) 22 × 22 cm^2, 3 mm slice thickness, 128 × 128 matrix, b = 0, 1000 s/mm^2 and 40 slices covering the whole brain. FLAIR images were obtained after a loading dose of 3ml gadodiamide contrast agent (Omniscan, GE Healthcare AS, Oslo, Norway). Post contrast T1-weighted MPRAGE images were acquired after administration of a standard dose (0.1 mmol/kg) of gadodiamide with a power injector (Medrad, Idianola, PA).

Image processing

All the diffusion images were analyzed off-line. The SNR was calculated from the non-diffusion weighted images and was computed by measuring the ratio of the image intensity from the brain and the standard division of the background noise (Farrell et al., 2007). Regions of interest (ROI) (90–110 pixels) were placed in the normal white matter (WM) (centrum semiovale), gray matter (parietal cortex) and background, followed by the calculation of SNR. The diffusion-weighted images were co-registered to the non-diffusion weighted (b = 0) images to minimize the artifacts induced by eddy-current and/or subject motion using a 3D affine transformation estimated by maximizing the mutual information between the images (Maes et al., 1997). The corrected raw images were combined to estimate rotationally invariant DTI parameter maps using DTI Studio (Version 2.4, H. Jiang, S. Mori, John Hopkins University). Pixel-wise ADC, FA, CL and CP maps were computed using the following equations.

$$\mathrm{ADC}=(\lambda_1+\lambda_2+\lambda_3)/3 \tag{1}$$

$$FA=\sqrt{\frac{3}{2}}\sqrt{\frac{(\lambda_1-\bar{\lambda})^2+(\lambda_2-\bar{\lambda})^2+(\lambda_3-\bar{\lambda})^2}{\lambda_1{}^2+\lambda_2{}^2+\lambda_3{}^2}} \tag{2}$$

$$CL=(\lambda_1-\lambda_2)/\sqrt{\lambda_1^2+\lambda_2^2+\lambda_3^2} \tag{3}$$

$$CP=2(\lambda_2 - \lambda_3)/\sqrt{\lambda_1^2+\lambda_2^2+\lambda_3^2} \quad (4)$$

where λ_1,λ_2 and λ_3 are the three eigenvalues of the diffusion tensor and denotes the mean of the three eigenvalues.

The scalar DTI maps (ADC, FA, CL, and CP) and FLAIR images were co-registered to CE T1-weighted images using a 3D non-rigid transformation and mutual information by combining affine transformation and discrete sine bases (Ashburner and Friston, 1999) up to 2nd order, depending on the degree of misalignment, determined by a neuroradiologist (SW).

A semi-automatic segmentation method was used to subdivide each lesion into four regions: central, enhancing, immediate peritumoral and distant peritumoral, based on the CE T1-weighted and FLAIR images as shown in Fig. 1A and B, respectively. One ROI was drawn over the FLAIR abnormality on every slice by a neuroradiologist (SW) to create a 3D composite mask. Similarly, another mask was manually drawn on the CE T1-weighted images for the contra-lateral normal WM. Once these two ROIs were available, the total abnormal area was automatically segmented into the above mentioned four subregions The enhancing region (ER) was defined as the region with enhancement higher than mean + 3SD of the signal intensity from the WM. The nonenhancing areas or regions with enhancement lower than mean + 3SD of the signal intensity from the WM inside the enhancing region were defined as the central region (CR). The immediate peritumoral region (IPR) was arbitrarily chosen as a 4 mm-wide band around the enhancing region to make it similar in width as the enhancing region. The remaining region of FLAIR abnormality, outside of the IPR, was defined as the distant peritumoral region (DPR). An example of these four regions is shown in Fig. 1C. This method of segmentation was successfully applied to all patients.

The CE T1 weighted images were normalized to the signal intensity of the contra-lateral normal WM. The median values of DTI metrics as well as the normalized signal intensity from the CE T1 weighted images in each region were measured from the solitary lesions in all patients. Data analysis tools including image co-registration and segmentation were implemented using IDL routines (ITT Visual Information Solutions, Boulder, CO). As FLAIR images were acquired after a preloading dose of gadodiamide, thereby having a potential T1 contribution, they were only used for ROI placement.

Statistical Analysis

The difference between glioblastomas and brain metastases was assessed for each region and image parameter maps using a Mann-Whitney U test. A p-value of less than 0.05 was considered significant. A cutoff value for each parameter was estimated by maximizing the sum of sensitivity and specificity. The efficacy of each parameter in all four regions for the classification was evaluated using a univariate logistic regression analysis. The parameters with a high predictive power ($p < 0.20$, Wald test) were selected and fed into a multivariate logistic regression analysis to determine the most significant parameters and to build an optimal logistic regression model (LRM) to classify glioblastomas and brain metastases. Model fit was evaluated by means of the Hosmer-Lemeshow goodness-of-fit test (Lemeshow and Hosmer, 1982). Areas under the receiver operating characteristic (ROC) curves (AUC) were computed using the selected parameters, combination of DTI parameters and LRM output. All data analysis was conducted using SPSS (SPSS for Windows, version 15.0; SPSS Inc., Chicago, Ill).

Results

The SNR, computed from the non-diffusion weighted images (b = 0) of all patients, were 84.91 ± 54.10 and 100.95 ± 56.66 for the white and gray matter regions. Representative images of a patient with glioblastoma are shown in Fig. 2. Conventional CE T1-weighted (Fig. 2A) and FLAIR images (Fig. 2B) showed ring enhancement and extensive edema. The ADC map (Fig. 2C) demonstrated restricted diffusion from the enhancing part, which also exhibited low anisotropy relative to the normal WM as evidenced from the three anisotropy maps shown in Fig. 2D–F. Figure 3 shows representative images of a patient with a metastatic brain mass from a primary lung adenocarcinoma. The lesion on conventional CE T1-weighted and FLAIR images and ADC maps (Fig 3A–C) looks similar compared with glioblastoma. But the tumor from the enhancing part appeared to have a lower anisotropy (Fig. 3D–F) in comparison to the glioblastoma shown in Fig. 2. A capsule-like ring in the boundary surrounding the tumors was observed in the CP maps in 25 out of 38 glioblastomas (66%), and in 15 out of 25 brain metastases (60%).

Comparison of imaging parameters between glioblastomas and brain metastases

A region wise comparison of the two tumor types using the segmented ROIs is shown in Fig. 4. There was no significant difference in the signal intensity of the CE T1-weighted images between the two tumors from either one of the segmented areas. Similarly, the median ADC values were also not significantly different between the two groups in all ROIs. In contrast, the median FA values showed significant differences from all four regions ($p < 0.001$ for CR, ER, IPR, and $p < 0.05$ for DPR). FA of glioblastomas from the ER was about 34% higher than that of the brain metastases and this difference was the largest in ER region as compared to the other segmented areas. CL values also showed significant differences ($p < 0.001$ for CR, ER, and IPR) between glioblastomas and metastases except in the DPR region ($p = 0.18$). The CL value of glioblastomas from the ER was about 36 % higher than that of the brain metastases. CP values showed significant differences from all four regions ($p < 0.001$ for ER, $p < 0.05$ for CR, IPR and DPR) and were about 24% higher from the ER in glioblastomas than that in metastases.

Discrimination model based on statistical analysis

Univariate analyses were performed for all parameters from each segmented area in order to select the ones with high predictive power ($p < 0.20$, Wald test). Each parameter with a significant difference was evaluated for its discriminative ability using ROC analysis as shown in Table 2. FA from the ER (AUC = 0.903) was the single best parameter for the classification, followed by CL (AUC = 0.898) and CP (AUC = 0.80). The selected parameters were then used for a multivariate logistic regression analysis with forward stepwise selection. The results indicated that the best LRM for the probability of glioblastomas was achieved with three parameters (ADC, FA and CP) from the ER as follows:

$$f(ADC,FA,CP)=\frac{1}{1+\exp(-(\beta_0+\beta_1 ADC+\beta_2 FA+\beta_3 CP))}$$

where $\beta_0 = -39.81$, $\beta_1 = 21.82$, $\beta_2 = 268.55$, and $\beta_3 = -160.65$. The Hosmer-Lemeshow test did not reveal any departure from fit ($p = 0.92$). Fig. 5 shows the ROC curves for DTI parameters from the ER and best LRM. The LRM of the three parameters (ADC, FA and CP) was more accurate than individual parameters alone with a cutoff value = 0.72, sensitivity = 92%, specificity = 100 % and AUC = 0.98. The AUC for combination of all four DTI parameters (FA, ADC, CL and CP) and commonly used parameters (FA and ADC) from ER were 0.98 and 0.96, respectively. A scatter plot of FA and ADC of the ER is shown in Fig. 6. ADC alone

was a poor discriminator (AUC = 0.57), however, when combined with FA, the differentiation between glioblastomas and metastases improved significantly (AUC = 0.96).

Discussion

In this study, we investigated the feasibility of using DTI metrics to differentiate glioblastomas from solitary brain metastases and demonstrate that FA, CL and CP exhibit significant differences between the two neoplasms in all four segmented regions (studied). The ROC analysis showed that FA and CL from the ER have the highest prediction accuracy when used alone. A multivariate logistic regression analysis revealed that the best classifier of these two tumor types is a LRM based ADC, FA and CP from the ER with 92% sensitivity and 100% specificity. These results suggest that the proposed analysis of DTI metrics improves the differentiation between glioblastomas and solitary brain metastases.

FA in the enhancing region of tumor

We observed higher FA values from the enhancing part of glioblastomas. FA reflects the orientation of tissue microstructure, which may not be limited to the WM tracts alone (Beaulieu, 2002). Higher anisotropy values have also been reported in brain abscess (Wang et al., 2006), glioblastomas (Beppu et al., 2003; Beppu et al., 2005) and areas of hemorrhage (Haris et al., 2006), indicating that FA is related to structural orientation of the tissue/cells in the imaging voxel (Haris et al., 2006). The relationship between FA and tumor cellularity is controversial, as both positive (Beppu et al., 2003; Beppu et al., 2005; Kinoshita et al., 2008) and negative (Stadlbauer et al., 2006) correlation has been reported. A possible reason for these conflicting reports could be the difference in the regions studied from the tumor. The enhancing region typically represents the solid part of the tumor, where normal brain fibers are almost completely destroyed or displaced by the tumor (Rees et al., 1996). On the other hand, in the non-enhancing part, FA is affected by both solid tumor and residual white matter. Even if tumor cellularity is the same in the enhancing and non-enhancing regions, FA will be higher in the non-enhancing part due to the presence of residual fibers (Kinoshita et al., 2008). The higher FA from the enhancing region of glioblastomas in the present study may be due to the fact that glioblastomas usually have higher cellularity than brain metastases (Altman et al., 2007; Carrier et al., 1994; Rees et al., 1996). An increase in the degree of directionality of water diffusion due to a decrease in extracellular volume (increased cellularity) may also induce increased FA values.

Shape of diffusion tensor in brain tumors

FA is a scalar metric, which provides the degree of anisotropy, but does not indicate the shape of the diffusion ellipsoid. While both CL and CP are responsible for increased FA, their relative values indicate the shape of diffusion ellipsoid (Alexander et al., 2000). The CL specifically highlights the region of tubular tensors and CP indicates regions of planar tensors (Westin et al., 2002; Zhang et al., 2006). We observed significantly higher CL values from the enhancing part of glioblastomas than metastasis. An earlier study also reported a decrease in CL from a patient with brain metastasis (Zhang et al., 2004). The difference in tensor shape values have also been used to differentiate between subtypes of meningiomas (Tropine et al., 2007). A recent study suggested that CL and CP can distinguish true from pseudo WM tracts inside the abscess cavity (Kumar et al., 2007). It has been reported that CL correlates with coherent neural fiber structures (Alexander et al., 2000; Zhang et al., 2004). These studies and our results indicate that CL and CP values provide additional information about tumor diffusion characteristics, which may further assist in differentiation of neoplasms. We also observed a capsule-like ring on the CP maps of some glioblastomas and metastases. This feature has also been reported in metastasis and mengingiomas (Tropine et al., 2007; Zhang et al., 2004). These reports and our findings suggest that the ring structure with high CP is non-specific and its

presence may simply due to the compression of surrounding tissue (Tropine et al., 2007; Zhang et al., 2004).

DTI and tumor infiltration

Earlier DTI studies on differentiation of glioblastomas from metastases have focused on the peritumoral regions with a hypothesis that these regions can demonstrate infiltration of glioblastomas into the normal brain parenchyma in comparison to the non-infiltrating metastatic brain lesions (Lu et al., 2003; Lu et al., 2004; Morita et al., 2005; Tsuchiya et al., 2005; Zhang and Olsson, 1997). Lu et al (Lu et al., 2004) reported a significant difference between tumor-infiltrated edema and pure vasogenic edema using a parameter called “tumor infiltration index” and also reported increased ADC in metastasis compared to glioblastomas. However, another study demonstrated reduced ADC in the peritumoral region of metastases compared to that of glioblastomas (Morita et al., 2005). The discrepancy between these studies may be due to the difference in the selection of ROIs for the peritumoral region. There have been a number of studies that focus on the area close to the enhancing region by either manually placing a number of small ROIs around the tumor (Lu et al., 2003; Morita et al., 2005) or by using a band of arbitrarily chosen thickness (e.g. 10 mm) around the tumor (Law et al., 2002; Oh et al., 2005). In the present study, we employed a semi-automatic segmentation technique to separate different regions of the tumor and peritumoral edema. The peritumoral areas were further subdivided into IPR and DPR as IPR may have a higher degree of tumor infiltration in comparison to DPR in glioblastomas. In the IPR, we observed a significant difference in FA, CL, and CP between glioblastomas and metastases. In the DPR, only FA and CP measurements reached significant difference between the two tumor types. While statistical significance was observed, the overall sensitivity, specificity and accuracy for all the measurements in the peritumoral areas were lower than in the enhancing part of the tumor. Since the edematous region contains areas of increased extra- and intracellular water, tumor infiltration and varying fractional composition of normal white/gray matter, it is difficult to determine which factor is reflected in DTI metrics. This might further explain the conflicting reports of DTI characteristics in these regions. In the absence of a true histopathological correlation, it is difficult to determine the true physiological boundaries of IPR and DPR. However, we believe that an arbitrarily chosen area of a defined thickness provides an objective and nonbiased approach for selecting a region with high likelihood of tumor infiltration. Future studies may be necessary to further optimize this selection method, in parallel with histopathological study.

Combined DTI metrics for classification

In our study, mutivariate logistic regression analysis allowed us to determine the best model that can differentiate glioblastomas from brain metastases. We observed that the combination of ADC, FA and CP from the enhancing part is the most powerful predictor for tumor classification, with a sensitivity of 92%, specificity of 100% and AUC 0.98. Combination of all the DTI parameters including FA, ADC, CL and CP did not improve the accuracy (AUC = 0.98). The accuracy of the commonly used metrics, FA and ADC was less than the LRM. Our results showed higher sensitivity than previously reported studies using FLAIR (44%) (Tang et al., 2006), perfusion-weighted imaging (69%) (Cha et al., 2007) or MR spectroscopy (80%) (Opstad et al., 2004) for differentiation of glioblastomas from brain metastases.

The current study is limited in ability to pinpoint the causes for the altered FA, CL and CP in tumors with respect to tissue composition, such as cellularity, vascularity, edema, tumor cell size and pattern of flowing blood in capillaries as image guided biopsy/surgery was not performed. Future studies in which specific radiologic-pathologic correlation is performed, will be necessary to precisely determine the reason for increased FA, ADC and CP in these tumors. As perfusion-weighted imaging and MR spectroscopy has also been used to differentiate between glioblastomas and metastases, though less accurate (Cha et al., 2007;

Law et al., 2002, Opstad et al.,2004), we believe that future studies including relative cerebral blood volume (rCBV) values and metabolite ratios in the LRM may further enhance the sensitivity of these methods in accurately identifying solitary enhancing lesions in the brain.

In conclusion, our results demonstrate that there is a significant ($p < 0.001$) difference in diffusion tensor anisotropy metrics (FA, CL and CP) of the enhancing parts of glioblastomas and metastases. These DTI metrics can be used individually or in combination, to differentiate glioblastomas from metastases. Further investigation with larger patient population and histological validation will be necessary to determine the robustness of these parameters in differentiating tumor types and increased understanding of morphological and functional characteristic of brain tumors.

Acknowledgements

NIH Grant RO1-CA102756

References

Alexander AL, Hasan K, Kindlmann G, Parker DL, Tsuruda JS. A geometric analysis of diffusion tensor measurements of the human brain. Magn Reson Med 2000;44:283–291. [PubMed: 10918328]

Altman DA, Atkinson DS Jr, Brat DJ. Best cases from the AFIP: glioblastoma multiforme. Radiographics 2007;27:883–888. [PubMed: 17495298]

Ashburner J, Friston KJ. Nonlinear spatial normalization using basis functions. Hum Brain Mapp 1999;7:254–266. [PubMed: 10408769]

Beaulieu C. The basis of anisotropic water diffusion in the nervous system - a technical review. NMR Biomed 2002;15:435–455. [PubMed: 12489094]

Beppu T, Inoue T, Shibata Y, Kurose A, Arai H, Ogasawara K, Ogawa A, Nakamura S, Kabasawa H. Measurement of fractional anisotropy using diffusion tensor MRI in supratentorial astrocytic tumors. J Neurooncol 2003;63:109–116. [PubMed: 12825815]

Beppu T, Inoue T, Shibata Y, Yamada N, Kurose A, Ogasawara K, Ogawa A, Kabasawa H. Fractional anisotropy value by diffusion tensor magnetic resonance imaging as a predictor of cell density and proliferation activity of glioblastomas. Surg Neurol 2005;63:56–61. [PubMed: 15639528]

Calli C, Kitis O, Yunten N, Yurtseven T, Islekel S, Akalin T. Perfusion and diffusion MR imaging in enhancing malignant cerebral tumors. Eur J Radiol 2006;58:394–403. [PubMed: 16527438]

Carrier DA, Mawad ME, Kirkpatrick JB, Schmid MF. Metastatic adenocarcinoma to the brain: MR with pathologic correlation. AJNR Am J Neuroradiol 1994;15:155–159. [PubMed: 8141048]

Cha S. Update on brain tumor imaging: from anatomy to physiology. AJNR Am J Neuroradiol 2006;27:475–487. [PubMed: 16551981]

Cha S, Lupo JM, Chen MH, Lamborn KR, McDermott MW, Berger MS, Nelson SJ, Dillon WP. Differentiation of glioblastoma multiforme and single brain metastasis by peak height and percentage of signal intensity recovery derived from dynamic susceptibility-weighted contrast-enhanced perfusion MR imaging. AJNR Am J Neuroradiol 2007;28:1078–1084. [PubMed: 17569962]

Farrell JA, Landman BA, Jones CK, Smith SA, Prince JL, van Zijl PC, Mori S. Effects of signal-to-noise ratio on the accuracy and reproducibility of diffusion tensor imaging-derived fractional anisotropy, mean diffusivity, and principal eigenvector measurements at 1.5 T. J Magn Reson Imaging 2007;26:756–767. [PubMed: 17729339]

Field AS, Alexander AL, Wu YC, Hasan KM, Witwer B, Badie B. Diffusion tensor eigenvector directional color imaging patterns in the evaluation of cerebral white matter tracts altered by tumor. J Magn Reson Imaging 2004;20:555–562. [PubMed: 15390227]

Giese A, Westphal M. Treatment of malignant glioma: a problem beyond the margins of resection. J Cancer Res Clin Oncol 2001;127:217–225. [PubMed: 11315255]

Haris M, Gupta RK, Husain N, Hasan KM, Husain M, Narayana PA. Measurement of DTI metrics in hemorrhagic brain lesions: possible implication in MRI interpretation. J Magn Reson Imaging 2006;24:1259–1268. [PubMed: 17096394]

Kim S, Pickup S, Hsu O, Poptani H. Diffusion tensor MRI in rat models of invasive and well-demarcated brain tumors. NMR Biomed 2007;21:208–216. [PubMed: 17530617]

Kinoshita M, Hashimoto N, Goto T, Kagawa N, Kishima H, Izumoto S, Tanaka H, Fujita N, Yoshimine T. Fractional anisotropy and tumor cell density of the tumor core show positive correlation in diffusion tensor magnetic resonance imaging of malignant brain tumors. NeuroImage. 2008In press

Kumar M, Gupta RK, Nath K, Rathore RK, Bayu G, Trivedi R, Husain M, Prasad KN, Tripathi RP, Narayana PA. Can we differentiate true white matter fibers from pseudofibers inside a brain abscess cavity using geometrical diffusion tensor imaging metrics? NMR Biomed 2007;21:581–588. [PubMed: 18050359]

Law M, Cha S, Knopp EA, Johnson G, Arnett J, Litt AW. High-grade gliomas and solitary metastases: differentiation by using perfusion and proton spectroscopic MR imaging. Radiology 2002;222:715–721. [PubMed: 11867790]

Lemeshow S, Hosmer DW Jr. A review of goodness of fit statistics for use in the development of logistic regression models. Am J Epidemiol 1982;115:92–106. [PubMed: 7055134]

Louis DN, Ohgaki H, Wiestler OD, Cavenee WK, Burger PC, Jouvet A, Scheithauer BW, Kleihues P. The 2007 WHO classification of tumours of the central nervous system. Acta Neuropathol 2007;114:97–109. [PubMed: 17618441]

Lu S, Ahn D, Johnson G, Cha S. Peritumoral diffusion tensor imaging of high-grade gliomas and metastatic brain tumors. AJNR Am J Neuroradiol 2003;24:937–941. [PubMed: 12748097]

Lu S, Ahn D, Johnson G, Law M, Zagzag D, Grossman RI. Diffusion-tensor MR imaging of intracranial neoplasia and associated peritumoral edema: introduction of the tumor infiltration index. Radiology 2004;232:221–228. [PubMed: 15220505]

Maes F, Collignon A, Vandermeulen D, Marchal G, Suetens P. Multimodality image registration by maximization of mutual information. IEEE Trans Med Imaging 1997;16:187–198. [PubMed: 9101328]

Morita K, Matsuzawa H, Fujii Y, Tanaka R, Kwee IL, Nakada T. Diffusion tensor analysis of peritumoral edema using lambda chart analysis indicative of the heterogeneity of the microstructure within edema. J Neurosurg 2005;102:336–341. [PubMed: 15739563]

Oh J, Cha S, Aiken AH, Han ET, Crane JC, Stainsby JA, Wright GA, Dillon WP, Nelson SJ. Quantitative apparent diffusion coefficients and T2 relaxation times in characterizing contrast enhancing brain tumors and regions of peritumoral edema. J Magn Reson Imaging 2005;21:701–708. [PubMed: 15906339]

Opstad KS, Murphy MM, Wilkins PR, Bell BA, Griffiths JR, Howe FA. Differentiation of metastases from high-grade gliomas using short echo time 1H spectroscopy. J Magn Reson Imaging 2004;20:187–192. [PubMed: 15269942]

Rees JH, Smirniotopoulos JG, Jones RV, Wong K. Glioblastoma multiforme: radiologic-pathologic correlation. Radiographics 1996;16:1413–1438. [PubMed: 8946545]

Rumboldt Z, Camacho DL, Lake D, Welsh CT, Castillo M. Apparent diffusion coefficients for differentiation of cerebellar tumors in children. AJNR Am J Neuroradiol 2006;27:1362–1369. [PubMed: 16775298]

Schiff D. Single Brain Metastasis. Curr Treat Options Neurol 2001;3:89–99. [PubMed: 11123862]

Soffietti R, Ruda R, Mutani R. Management of brain metastases. J Neurol 2002;249:1357–1369. [PubMed: 12382150]

Stadlbauer A, Ganslandt O, Buslei R, Hammen T, Gruber S, Moser E, Buchfelder M, Salomonowitz E, Nimsky C. Gliomas: histopathologic evaluation of changes in directionality and magnitude of water diffusion at diffusion-tensor MR imaging. Radiology 2006;240:803–810. [PubMed: 16926329]

Tang YM, Ngai S, Stuckey S. The solitary enhancing cerebral lesion: can FLAIR aid the differentiation between glioma and metastasis? AJNR Am J Neuroradiol 2006;27:609–611. [PubMed: 16552003]

Tropine A, Dellani PD, Glaser M, Bohl J, Ploner T, Vucurevic G, Perneczky A, Stoeter P. Differentiation of fibroblastic meningiomas from other benign subtypes using diffusion tensor imaging. J Magn Reson Imaging 2007;25:703–708. [PubMed: 17345634]

Tsuchiya K, Fujikawa A, Nakajima M, Honya K. Differentiation between solitary brain metastasis and high-grade glioma by diffusion tensor imaging. Br J Radiol 2005;78:533–537. [PubMed: 15900059]

Wang S, Wolf RL, Woo JH, Wang J, O'Rourke DM, Roy S, Melhem ER, Poptani H. Actinomycotic brain infection: registered diffusion, perfusion MR imaging and MR spectroscopy. Neuroradiology 2006;48:346–350. [PubMed: 16614822]

Westin CF, Maier SE, Mamata H, Nabavi A, Jolesz FA, Kikinis R. Processing and visualization for diffusion tensor MRI. Med Image Anal 2002;6:93–108. [PubMed: 12044998]

Westin CF, Peled S, Gubjartsson H, Kikinis R, Jolesz FA. Geometrical Diffusion Measures for MRI from tensor Basis Analysis. Proceedings of ISMRM 1997:1–72.

Yamasaki F, Kurisu K, Satoh K, Arita K, Sugiyama K, Ohtaki M, Takaba J, Tominaga A, Hanaya R, Yoshioka H, Hama S, Ito Y, Kajiwara Y, Yahara K, Saito T, Thohar MA. Apparent diffusion coefficient of human brain tumors at MR imaging. Radiology 2005;235:985–991. [PubMed: 15833979]

Zhang J, van Zijl PC, Mori S. Image contrast using the secondary and tertiary eigenvectors in diffusion tensor imaging. Magn Reson Med 2006;55:439–449. [PubMed: 16402380]

Zhang M, Olsson Y. Hematogenous metastases of the human brain--characteristics of peritumoral brain changes: a review. J Neurooncol 1997;35:81–89. [PubMed: 9266444]

Zhang S, Bastin ME, Laidlaw DH, Sinha S, Armitage PA, Deisboeck TS. Visualization and analysis of white matter structural asymmetry in diffusion tensor MRI data. Magn Reson Med 2004;51:140–147. [PubMed: 14705054]

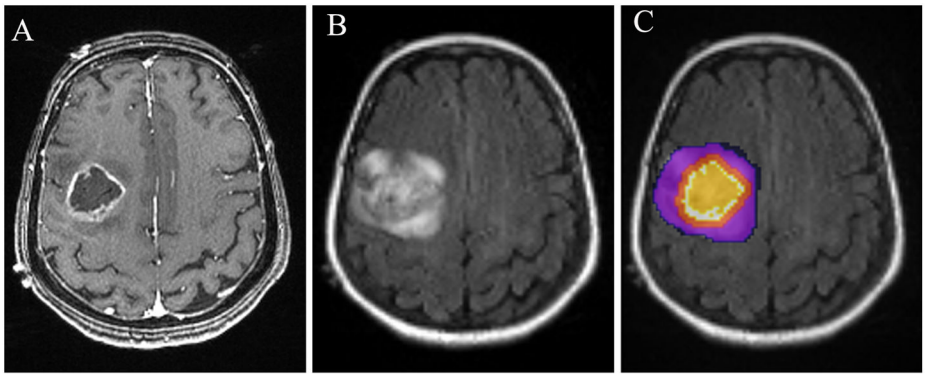

Figure 1.
Region of interest (ROI) placement in a patient with glioblastoma. Transverse contrast-enhanced T1-weighted (A) and FLAIR (B) images showing a ring-enhancing lesion in the right frontal lobe. ROIs are overlayed on FLAIR image with the colors indicating the following defined regions: orange, central region; white, enhancing region; red, immediate peritumoral region; purple, distant peritumoral region (C).

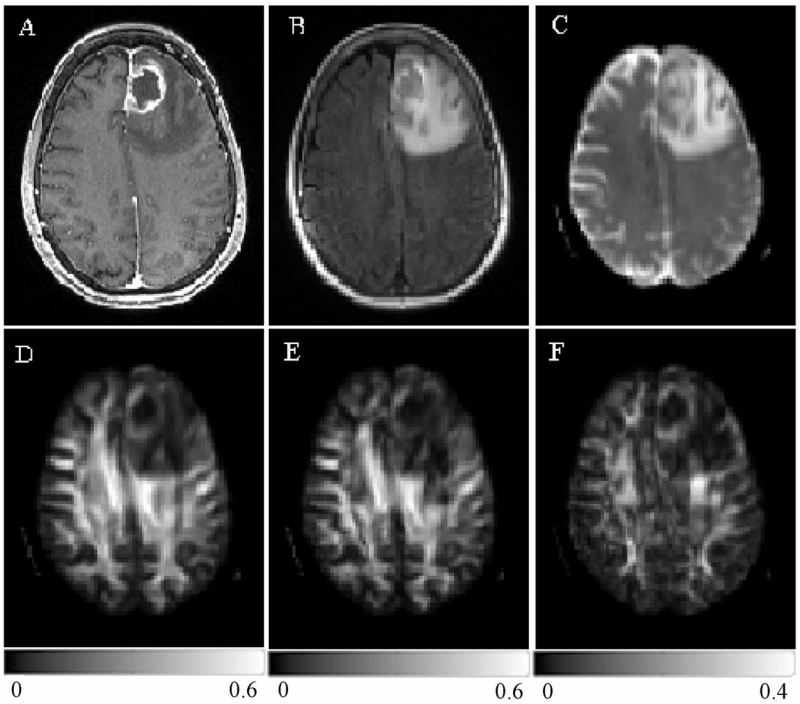

Figure 2.

A 68 year old female with a glioblastoma in the left frontal lobe. There was no hemorrhage based on T1 and T2-weighted images (not shown). Transverse contrast-enhanced T1-weighted (A) and FLAIR (B) images show ring-enhancement and extensive edema. ADC map (C) shows restricted diffusion of the enhancing part. FA (D), CL (E) and CP (F) from the enhancing part are lower than normal appearing white matter, but higher than that for brain metastases (Figure 3).

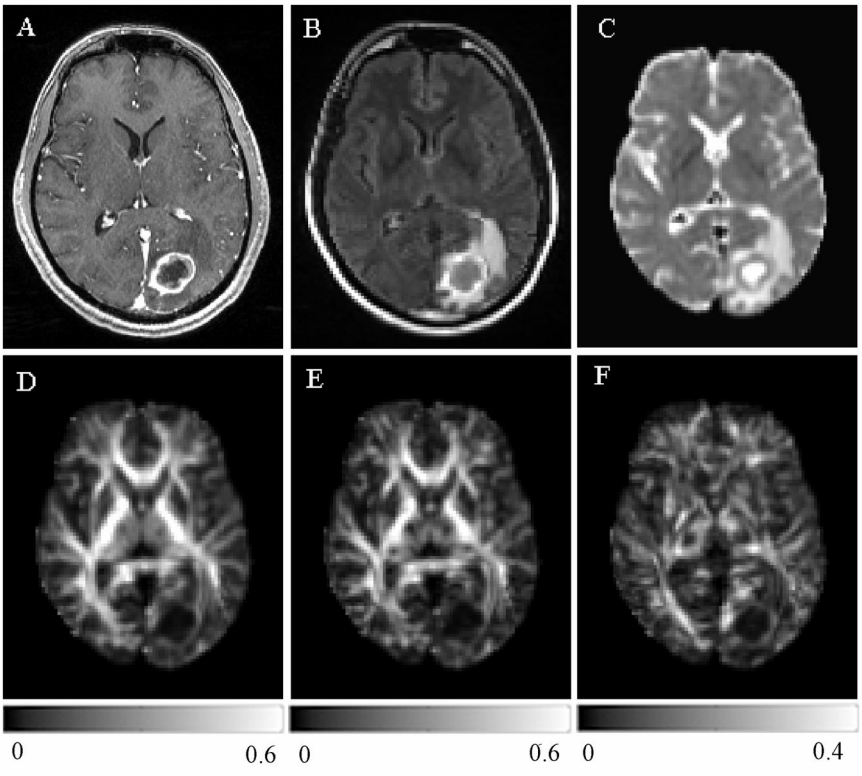

Figure 3.

A 56 year old male with metastatic lung adenocarcinoma in the left occipital lobe. There was no hemorrhage based on T1 and T2-weighted images (not shown). Transverse contrast-enhanced T1-weighted (A) and FLAIR (B) images show a ring-enhancing lesion with extensive edema, similar in appearance to the glioblastoma shown in Figure 2 (A and B). ADC map (C) shows restricted diffusion of the enhancing part. Lower FA (D), CL (E) and CP (F) are noticed from the enhancing part relative to normal appearing white matter compared with the glioblastoma.

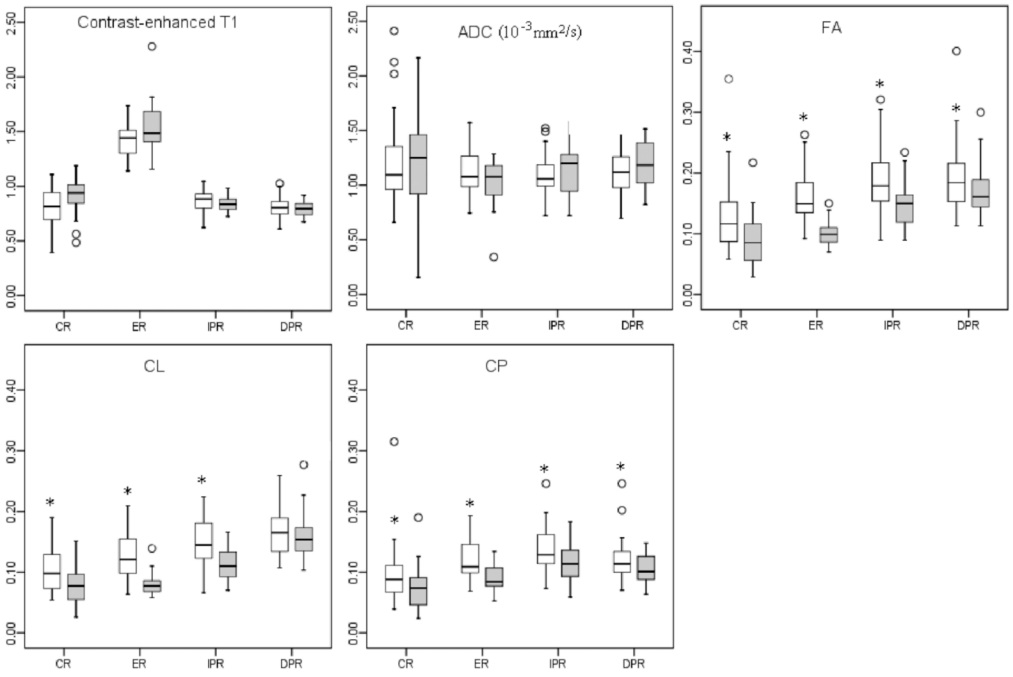

Figure 4.

Box plot of imaging characteristics in glioblastomas (white box) and brain metastases (gray box). Boxes represent the 25th and 75th percentiles with the medians indicated by the middle lines in the boxes. Vertical bars (whiskers) indicate the range of data except the outliers (values more than 1.5 times of the box length larger than the 75th percentile or smaller than the 25th percentile) represented by circles. * indicates significant differences ($p < 0.05$) between glioblastomas and brain metastases. CR: central region. ER: enhancing region. IPR: immediate peritumoral region. DPR: distant peritumoral region

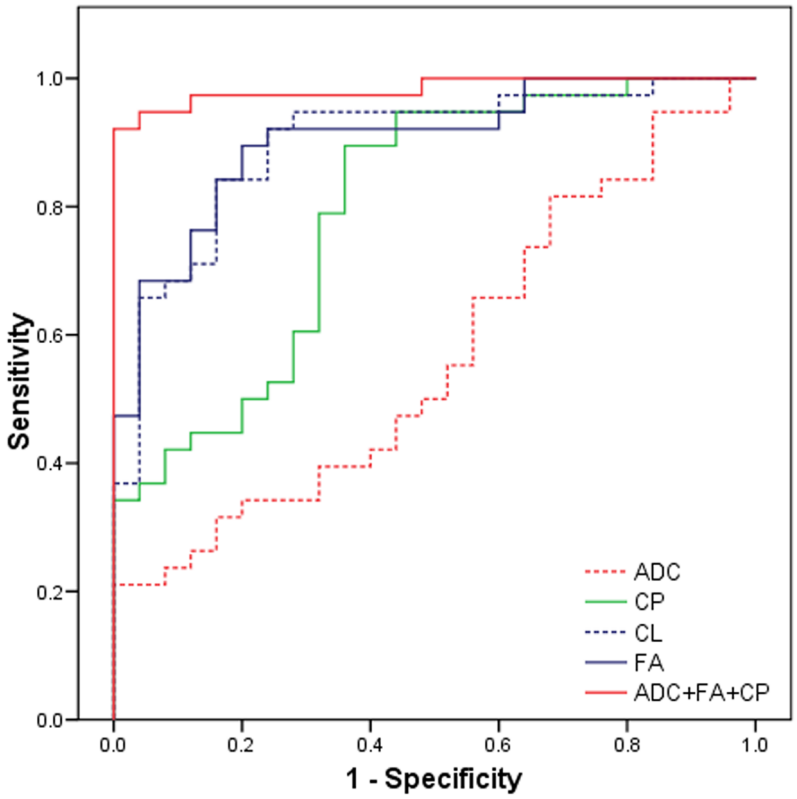

Figure 5.
Receiver operative characteristic (ROC) curves for FA, CL, CP, ADC and ADC+FA+CP from the enhancing region of the tumor. ADC+FA+CP is the best predictor for differentiation of glioblastomas from brain metastases with area under the curve (AUC) 0.98.

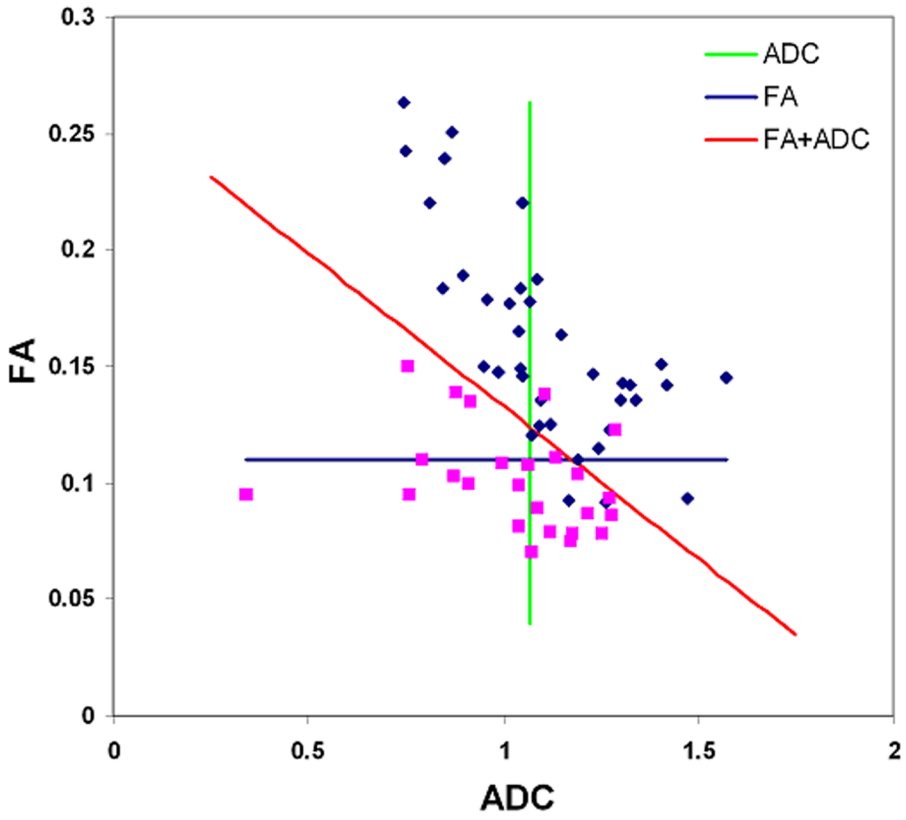

Figure 6.
Scatter plot of FA and ADC from the enhancing region of glioblastomas (blue square) and brain metastases (purple square). The vertical green line is the cutoff line for ADC (cutoff value = 1.07 as shown in Table 2), which does not separate glioblastomas from metastases well enough. The horizontal blue line is the cutoff line for FA (cutoff value = 0.11 as in Table 2), which separates glioblastomas from metastases better than ADC. The diagonal red line is the cutoff line for the combined model of FA and ADC, which divides glioblastomas and metastases much better than FA or ADC alone.

Table 1

Primary sites of cancer for patients with brain metastases

Site	No. of patients
Lung	11
Breast	6
Melanoma	5
Colon	1
Parotid	1
Esophagus	1

Table 2

Sensitivity and specificity of imaging parameters with high predictive power ($p < 0.20$, Wald test) in differentiation of glioblastomas from brain metastases using receiver operating characteristic curve analysis

Parameter	ROI	Cutoff value	Sensitivity	Specificity	AUC
CE T1	CR	0.84	0.42	0.24	0.33
	ER	1.42	0.58	0.44	0.39
ADC($10^{-3}mm^2/s$)	ER	1.07	0.55	0.48	0.57
FA	CR	0.10	0.71	0.68	0.72
	ER	0.11	0.89	0.80	0.90
	IPR	0.16	0.66	0.76	0.74
	DPR	0.17	0.68	0.60	0.63
CL	CR	0.10	0.47	0.88	0.71
	ER	0.09	0.84	0.84	0.90
	IPR	0.13	0.66	0.76	0.76
CP	CR	0.05	0.92	0.36	0.66
	ER	0.09	0.90	0.64	0.80
	IPR	0.12	0.76	0.52	0.66
	DPR	0.10	0.78	0.48	0.63

Note - CE T1: contrast-enhanced T1 AUC: area under the curve

CR: central region.

ER: enhancing region.

IPR: immediate peritumoral region

DPR: distant peritumoral region